The Astrophysical Journal Letters, 725:L62–L67, 2010 December 10 doi:10.1088/2041-8205/725/1/L62

THE RELATIONSHIP BETWEEN MOLECULAR GAS AND STAR FORMATION IN LOW-MASS E/S0 GALAXIES

Lisa H. Wei[1], Stuart N. Vogel[1], Sheila J. Kannappan[2], Andrew J. Baker[3], David V. Stark[2], and Seppo Laine[4]
[1] Department of Astronomy, University of Maryland, College Park, MD 20742-2421, USA
[2] Department of Physics and Astronomy, University of North Carolina, Phillips Hall CB 3255, Chapel Hill, NC 27599-3255, USA
[3] Department of Physics and Astronomy, Rutgers, the State University of New Jersey, 136 Frelinghuysen Road, Piscataway, NJ 08854-8019, USA
[4] Spitzer Science Center, California Institute of Technology, MS 220-6, Pasadena, CA 91125, USA
Received 2010 August 18; accepted 2010 November 4; published 2010 November 19

ABSTRACT

We consider the relationship between molecular gas and star formation surface densities in 19 morphologically defined E/S0s with stellar mass $\lesssim 4 \times 10^{10}\ M_{\odot}$, paying particular attention to those found on the blue sequence in color versus stellar mass parameter space, where spiral galaxies typically reside. While some blue-sequence E/S0s must be young major-merger remnants, many low-mass blue-sequence E/S0s appear much less disturbed and may be experiencing the milder starbursts associated with inner-disk building as spirals (re)grow. For a sample of eight E/S0s (four blue, two mid, and two red sequence) whose CARMA CO(1–0), *Spitzer* MIPS 24 μm, and *GALEX* FUV emission distributions are spatially resolved on a 750 pc scale, we find roughly linear relationships between molecular gas and star formation surface densities within all galaxies, with power-law indices $N = 0.6$–1.9 (median 1.2). Adding 11 more blue-sequence E/S0s whose CO(1–0) emission is not as well resolved, we find that most of our E/S0s have global 1–8 kpc aperture-averaged molecular gas surface densities overlapping the range spanned by the disks and centers of spiral galaxies. While many of our E/S0s fall on the same Schmidt–Kennicutt relation as local spirals, ∼80% (predominantly on the blue sequence) are offset toward apparently higher molecular gas star formation efficiency (i.e., shorter molecular gas depletion time). Possible interpretations of the elevated efficiencies include bursty star formation similar to that in local dwarf galaxies, H_2 depletion in advanced starbursts, or simply a failure of the CO(1–0) emission to trace all of the molecular gas.

Key words: galaxies: elliptical and lenticular, cD – galaxies: evolution – galaxies: star formation

1. INTRODUCTION

Much progress has been made in recent decades in understanding the relationship between star formation rate surface density ($\Sigma_{\rm SFR}$), and gas surface density ($\Sigma_{\rm gas}$) in nearby star-forming spiral galaxies, and this work has been used to infer the physical basis of the star formation law (e.g., Krumholz et al. 2009; Murray 2009). Studies relating the two observables with a power law of the form

$$\Sigma_{\rm SFR} = a\Sigma_{\rm gas}^{N}, \quad (1)$$

typically find power-law indices N ranging from 1 to 3 (e.g., Kennicutt 1998; Wong & Blitz 2002; Kennicutt et al. 2007; see Bigiel et al. 2008 for a review of previous work). In a spatially resolved study of H I and H_2 in star-forming spirals, Bigiel et al. (2008) find a linear ($N \sim 1$) relation between $\Sigma_{\rm SFR}$ and molecular gas surface density ($\Sigma_{\rm H_2}$), but little to no correlation between $\Sigma_{\rm SFR}$ and H I surface density.

In contrast, less is known about the connection between $\Sigma_{\rm gas}$ and star formation in early-type galaxies. The good correlation between the morphologies of molecular gas, 24 μm emission, and radio continuum in local E/S0s hints that there is a relationship between $\Sigma_{\rm H_2}$ and $\Sigma_{\rm SFR}$ (Young et al. 2009). In a single-dish survey of CO emission in SAURON E/S0s, Combes et al. (2007) find that their galaxies follow the $N = 1.4$ disk-averaged power law, characteristic of spirals (Kennicutt 1998). Using multiple star formation tracers, Crocker et al. (2010) find a similar result for a sample of 12 E/S0s, although possibly at lower total gas star formation efficiencies (TSFE ≡ $\rm SFR/M_{HI+H_2+He}$). Shapiro et al. (2010) update the Combes et al. results with spatially resolved maps, localizing both CO emission and star formation in the central regions of the galaxies and finding $\Sigma_{\rm SFR}$, $\Sigma_{\rm H_2}$, and molecular gas star formation efficiency (MSFE ≡ $\rm SFR/M_{H_2+He}$) values similar to those of spirals. However, spatially resolved studies of the H_2–star-formation relation at sub-kpc resolution similar to the analyses of Kennicutt et al. (2007) and Bigiel et al. (2008) have yet to be done for E/S0s.

Recent work has identified a local population of star-forming E/S0s that reside alongside spirals on the blue sequence in color versus stellar mass space (Kannappan et al. 2009, hereafter KGB). The fraction of E/S0s on the blue sequence increases with decreasing mass, from $\gtrsim$5% at stellar mass $M_* \sim 3\times10^{10}\ M_{\odot}$ up to $\gtrsim$20%–30% for $M_* \lesssim 5\times10^{9}\ M_{\odot}$ (2% and 5%, respectively, of all galaxies in these mass ranges; KGB). High-mass blue-sequence E/S0s are often young major-merger remnants that will fade to the red sequence (see also Schawinski et al. 2009). Low-mass blue-sequence E/S0s, in contrast, appear more settled, occupying low-density field environments where gas accretion is likely (KGB). This population may reflect the transformation of "red and dead" E/S0s into spirals via inner- and outer-disk regrowth (KGB). KGB argue that many blue-sequence E/S0s occupy a "sweet spot" in M_* and stellar concentration index, characterized by abundant gas and bursty, efficient (when time averaged over multiple bursts) star formation, which may enable efficient disk building (see also Section 5). Wei et al. (2010) confirm that blue-sequence E/S0s have fractionally large atomic gas reservoirs, comparable to those of spirals (0.1–1.0, relative to M_*). The ongoing star formation and large gas reservoirs of these galaxies make them ideal for probing the spatially resolved relationship between $\Sigma_{\rm H_2}$ and $\Sigma_{\rm SFR}$ in E/S0s, offering unique insight into whether/how some E/S0s may be actively evolving via bursty, efficient star formation.

Table 1
Aperture-averaged Properties for CARMA and IRAM 30 m E/S0s

Galaxy	Seq.	D_{maj} (′)	Dist. (Mpc)	M_* (log $M_\odot$)	$M_{H\,I}$ (log $M_\odot$)	$M_{H_2,C}$ (log $M_\odot$)	$M_{H_2,S}$ (log $M_\odot$)	R_{ap} (″)	Inclin. (°)	Σ_{H_2} ($M_\odot$ pc^{-2})	Σ_{SFR} ($M_\odot$ yr^{-1} kpc^{-2})	τ_{dep} (Gyr)
NGC 3011	B	0.8	25.7	9.4	8.3		< 7.0	12.1	27	<1.2	0.007 ± 0.001	<0.22
NGC 3032	B	1.3	25.2	9.6	8.3	8.6	8.6[a]	10.6	26	61.1 ± 2.0	0.048 ± 0.002	1.74 ± 0.10
NGC 3073	B	1.1	21.1	9.1	8.5		7.0[b]	10.6	31	3.0 ± 0.6	0.004 ± 0.001	0.91 ± 0.27
UGC 6003	B	0.6	84.2	10.1	9.4	8.6	8.7	7.5	19	15.1 ± 1.4	0.087 ± 0.003	0.24 ± 0.02
IC 692	B	0.8	21.4	8.9	8.4		6.8	12.1	42	1.0 ± 0.3	0.006 ± 0.001	0.22 ± 0.08
UGC 6570*	M	1.2	28.6	9.6	8.4	8.0	8.0	7.5	62	10.1 ± 0.8	0.066 ± 0.001	0.21 ± 0.02
UGC 6637*	B	0.9	31.5	9.2	8.6		7.3	12.1	66	0.7 ± 0.2	0.004 ± 0.001	0.25 ± 0.07
NGC 3773	B	1.1	10.5	8.6	7.9	6.6		10.6	44	4.7 ± 0.6	0.058 ± 0.004	0.11 ± 0.02
NGC 3870	B	1.0	14.5	8.8	8.4	6.9	7.2[c]	12.1	41	3.3 ± 0.5	0.038 ± 0.003	0.12 ± 0.02
UGC 6805	B	0.7	20.3	8.9	7.6	7.6	7.4	9.0	45	10.5 ± 0.9	0.015 ± 0.001	0.96 ± 0.12
UGC 7020A	M	1.1	26.7	9.3	8.6	8.3	8.2	7.5	62	20.3 ± 1.2	0.048 ± 0.002	0.57 ± 0.04
NGC 4117	R	1.8	19.0	9.7	8.3	7.7		7.5	72	8.4 ± 0.6	0.005 ± 0.000	2.35 ± 0.25
NGC 5173	B	1.2	41.2	10.3	9.3	8.2		10.6	39	5.5 ± 0.6	0.006 ± 0.001	1.30 ± 0.23
NGC 5338	R	1.9	10.3	8.9	7.3	7.3	7.4[d]	7.5	57	19.0 ± 1.2	0.011 ± 0.001	2.27 ± 0.26
UGC 9562	B	0.9	25.2	8.9	9.3		7.0	12.1	68	0.9 ± 0.3	0.003 ± 0.001	0.37 ± 0.15
IC 1141	B	0.7	68.0	10.4	9.3	9.2		7.5	26	54.7 ± 2.7	0.078 ± 0.002	0.95 ± 0.06
NGC 7077[e]	B	0.9	18.9	8.8	8.2		7.1	10.6	40	3.3 ± 0.5	0.013 ± 0.002	0.35 ± 0.07
NGC 7360	B	1.2	67.9	10.5	9.6		< 7.8	12.1	67	<0.5	0.001 ± 0.000	<0.55
UGC 12265N	B	0.6	82.8	10.1	9.4	8.9	8.9	7.5	42	16.9 ± 1.3	0.049 ± 0.001	0.47 ± 0.04

Notes. Optical major axis (D_{maj}), M_*, and distance data are from KGB. H I data are from Wei et al. (2010), and references therein. $M_{H_2,C}$ is estimated from CARMA CO(1–0) data, and $M_{H_2,S}$ from single-dish data (central pointings only) from S. J. Kannappan et al. (2011, in preparation) and D. V. Stark et al. (2011, in preparation), except as marked: [a] Thronson et al. 1989; [b] Sage et al. 2007; [c] Welch & Sage 2003; [d] Leroy et al. 2005. $\tau_{dep} \equiv M_{H_2+He}/SFR$.
[e] Inclination assumed in calculating Σ_{H_2} and Σ_{SFR} is uncertain.

2. SAMPLE AND DATA

Our parent sample of 32 galaxies consists of all E/S0s (14 blue, 2 mid, and 11 red sequence) with $M_* \leqslant 4 \times 10^{10}\,M_\odot$ from the Nearby Field Galaxy Survey (NFGS; Jansen et al. 2000) and an additional five blue-sequence E/S0s in the same mass range (see KGB). The sample was defined for *Spitzer* and *GALEX* programs GO-30406 and GI3-046012 (PI: Kannappan), so all galaxies have new or archival FUV and 24 μm data for SFR estimation. Of the parent sample, we observed 23 E/S0s in CO(1–0) with the Combined Array for Research in Millimeter-Wave Astronomy (CARMA), detecting 12 of 23. In this Letter, we focus on the 12 E/S0s with CARMA detections and 7 additional E/S0s with IRAM 30 m observations (five detections, two limits) in CO(1–0). These 19 E/S0s sample a large range (Table 1) in color and stellar mass (Figure 1), H_2/H I mass ratio (0.006–3.2), and total gas-to-stellar mass ratio (0.07–3.4).

The CARMA maps have beam sizes of 2″–4″, with velocity coverage of 300–450 km s^{-1} and resolution of ∼2.5 km s^{-1}. We reduced the data with the MIRIAD package (Sault et al. 1995), using natural weighting. A more detailed description of the CARMA data reduction will be provided in L. Wei et al. (2011, in preparation). IRAM 30 m CO(1–0) observations are from S. J. Kannappan et al. (2011, in preparation) and D. V. Stark et al. (2011, in preparation), with additional literature data as noted in Table 1. We consider central pointings only, so the 23″ IRAM beam probes inner disks (relative to ∼0.′6–1.′9 optical diameters). Comparison between CARMA and IRAM 30 m fluxes suggests that little flux is resolved out by the interferometric observations.

We use the pipeline 24 μm mosaics from the *Spitzer* archive and the background-subtracted pipeline-processed FUV data from the *GALEX* archive. The CARMA and *GALEX* data sets were convolved with a kernel that reproduces the MIPS 24 μm point-spread function (FWHM ∼ 6″; Gordon et al. 2008) exactly in the CARMA/*GALEX* images, including the Airy ring, which is <1% of the $I_{24,peak}$. For our pixel-to-pixel analysis in Section 3, we further convolve our data to a resolution of 750 pc (6.″1–15.″3) for comparison with Bigiel et al. (2008). All maps are at least Nyquist sampled.

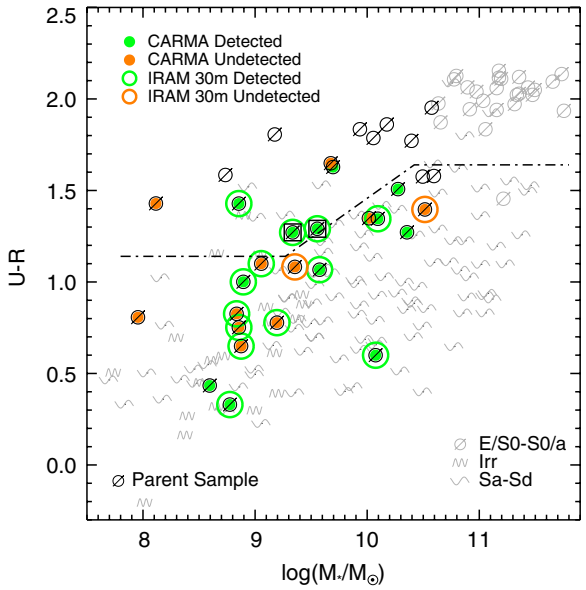

Figure 1. *U*−*R* color vs. stellar mass for galaxies in the NFGS (Jansen et al. 2000), plus five additional E/S0s from the literature. Symbols denote morphological types (KGB). The red sequence, i.e., the main locus of traditional red E/S0s, lies above the dashed line (with two borderline "mid sequence" E/S0s boxed, see KGB), while the blue sequence (typically populated by spirals) lies below. Dark symbols denote the 32 galaxies in the parent sample; the rest of the NFGS is shown in light gray.

We estimate Σ_{H_2} and Σ_{SFR} following Leroy et al. (2008):

$$\frac{\Sigma_{H_2}}{M_\odot\,\mathrm{pc}^{-2}} = 4.4\cos i\,\frac{I_{CO(1-0)}}{\mathrm{K\,km\,s}^{-1}} \quad (2)$$

$$\frac{\Sigma_{SFR}}{M_\odot\,\mathrm{kpc}^{-2}\,\mathrm{yr}^{-1}} = \cos i\,\frac{8.1\times10^{-2}\,I_{FUV}+3.2\times10^{-3}\,I_{24}}{\mathrm{MJy\,sr}^{-1}}, \quad (3)$$

assuming a CO-to-H_2 conversion factor (X_{CO}) of $2\times10^{20}\,\mathrm{cm}^{-2}$ $(\mathrm{K\,km\,s}^{-1})^{-1}$. Our estimates of Σ_{H_2} do not include helium; however, helium is included in estimates of molecular gas depletion time. Equation (3) uses the broken power-law initial mass function given by Kroupa (2001). Our procedures for calculating Σ_{H_2} and Σ_{SFR} are identical to those of Bigiel et al. (2008) after their conversion from CO(2–1) to CO(1–0) ($I_{CO(2-1)}/I_{CO(1-0)} = 0.8$), ensuring a fair comparison between the two data sets.

Active galactic nucleus (AGN) contamination is not an issue for the 750 pc resolution analysis, as any AGN contribution in the infrared would be contained within the central resolution element. NGC 4117 and IC 1141 are known AGN hosts, and optical line diagnostics from Kewley et al. (2006) identify NGC 5173 as a candidate host. However, IRAC color–color diagnostics (Sajina et al. 2005) suggest that (possible) AGN contributions to the integrated infrared emission in our galaxies are relatively weak, as the removal of the central resolution element does not significantly affect their positions in the infrared color–color diagram. Following Temi et al. (2007), we estimate possible 24 μm emission contamination from passively evolving stellar populations to be <8% for our E/S0s.

3. THE RESOLVED STAR FORMATION RELATION AT 750 pc RESOLUTION

Figure 2 plots the pixel-to-pixel relationship between Σ_{SFR} and Σ_{H_2} for the eight of our 19 galaxies resolved on 750 pc scales. We also include the 750 pc resolution data for the seven spirals observed by Bigiel et al. (2008) as light blue dots. The vertical dashed lines demarcate the three different star formation regimes discussed by Bigiel et al. (2008): H I-dominated, giant molecular cloud (GMC)/disk, and starburst. Figure 2 shows that all but two of the eight galaxies have some regions that fall within the GMC/disk regime, with two blue- and one mid-sequence E/S0s (NGC 3032, UGC 6570, and UGC 7020A) having the majority of their points in this regime.

We fit the Σ_{H_2}–Σ_{SFR} relationship with a power law of the form

$$\Sigma_{SFR} = a\left(\frac{\Sigma_{H_2}}{b\,M_\odot\,\mathrm{pc}^{-2}}\right)^N \quad (4)$$

in log–log space using the ordinary least-squares (OLS) bisector method (solid line in Figure 2) and list the fit parameters in Table 2, using coefficient $A = \log_{10}(a/M_\odot\,\mathrm{kpc}^{-2}\,\mathrm{yr}^{-1})$. Note that we set the intercept of our fit at $\log_{10}(b)$, where b is the median Σ_{H_2} for each galaxy, to lessen the effect of the covariance between N and A. The power-law index N ranges from 0.62 to 1.92, with a median of ∼1.2. It is evident that the majority of E/S0s in Figure 2 exhibit a power-law relation between Σ_{H_2} and Σ_{SFR}, all the way down to the H I-dominated regime.

Figure 2 also plots (dotted) lines of constant MSFE with $N = 1$, defined as the inverse of the molecular gas depletion time M_{H_2+He}/SFR, and illustrates variations in N and $M_{H_2}/M_{H\,I}$. For blue- and mid-sequence E/S0s, we find that as MSFE increases, N seems to steepen and $M_{H_2}/M_{H\,I}$ seems to decrease. We find a wider range of MSFEs (4%–70%) compared to the 3%–8% found by Bigiel et al. (2008). We discuss whether MSFE truly measures molecular gas star formation *efficiency* in Section 5.

Table 2
Star Formation Relation Fit Parameters

Galaxy	b ($M_\odot$ pc^2)	Coeff. A	Index N	rms (dex)
Blue sequence				
NGC 3032	33.7	-1.62 ± 0.02	1.10 ± 0.08	0.12
NGC 3773	1.7	-1.75 ± 0.07	1.24 ± 0.16	0.20
NGC 3870	2.7	-1.67 ± 0.06	1.92 ± 0.35	0.23
UGC 6805	7.1	-2.06 ± 0.03	1.19 ± 0.10	0.18
Mid sequence				
UGC 6570	11.7	-1.21 ± 0.06	1.20 ± 0.14	0.23
UGC 7020A	7.7	-1.73 ± 0.03	1.02 ± 0.08	0.21
Red sequence				
NGC 4117	3.0	-2.81 ± 0.02	1.10 ± 0.06	0.13
NGC 5338	5.2	-2.37 ± 0.03	0.62 ± 0.11	0.09
Median	7.1	−1.73	1.19	

4. THE GLOBAL STAR FORMATION RELATION

In Figure 3, we show the 1–8 kpc aperture-averaged relationship between Σ_{H_2} and Σ_{SFR} for the eight E/S0s of Figure 2 plus 11 more blue-sequence E/S0s with CARMA detections and/or IRAM observations as well as for normal spiral disk and starburst galaxies (Kennicutt 1998) and SAURON E/S0s (Shapiro et al. 2010). With the exception of Kennicutt's normal disk points, all the other points in Figure 3 show the surface densities within regions of star formation or molecular gas. The starbursts were averaged over "the radius of the starburst region" determined from CO/infrared imaging (Kennicutt 1998), and the SAURON E/S0s were averaged over the extent of the star-forming region defined by 8 μm polycyclic aromatic hydrocarbon emission (Shapiro et al. 2010). For our 19 E/S0s, we average M_{H_2} and SFR over an area with radius (R_{ap}) twice the scale length of the 24 μm emission, where the flux drops by e^{-2} from the peak. This area encompasses most of the flux in CO, 24 μm, and FUV, and corresponds well to the visual impression of the extent of CO emission for most galaxies. Note that the dots from Bigiel et al. (2008) plotted in the background for reference are *local* (750 pc) measures of Σ_{H_2} and Σ_{SFR} as in Figure 2.

In contrast, the Kennicutt (1998) spiral disk points are averaged over R_{25}, which may dilute the values of Σ_{H_2} and Σ_{SFR}. We infer this from radial profiles of normal spirals in Bigiel et al. (2008), which indicate that H_2 typically extends out to only ∼0.6 R_{25}. Thus, the surface densities calculated by Kennicutt (1998) for spiral disks should for consistency move up along lines of constant MSFE by ∼0.62 dex (gray arrow in Figure 3).

Comparison of these data sets reveals that the aperture-averaged Σ_{H_2} and Σ_{SFR} for our 19 E/S0s overlap the range spanned by spiral disks, with six of the CARMA-detected E/S0s having sufficiently high surface densities to occupy the same space where Kennicutt (1998) finds the *centers* of spirals lie—between normal disks and starburst galaxies (not shown in Figure 3, as Kennicutt tabulates only combined H I+H_2 data for galaxy centers). Our E/S0s also appear to span the same range as the typically more massive SAURON E/S0s.

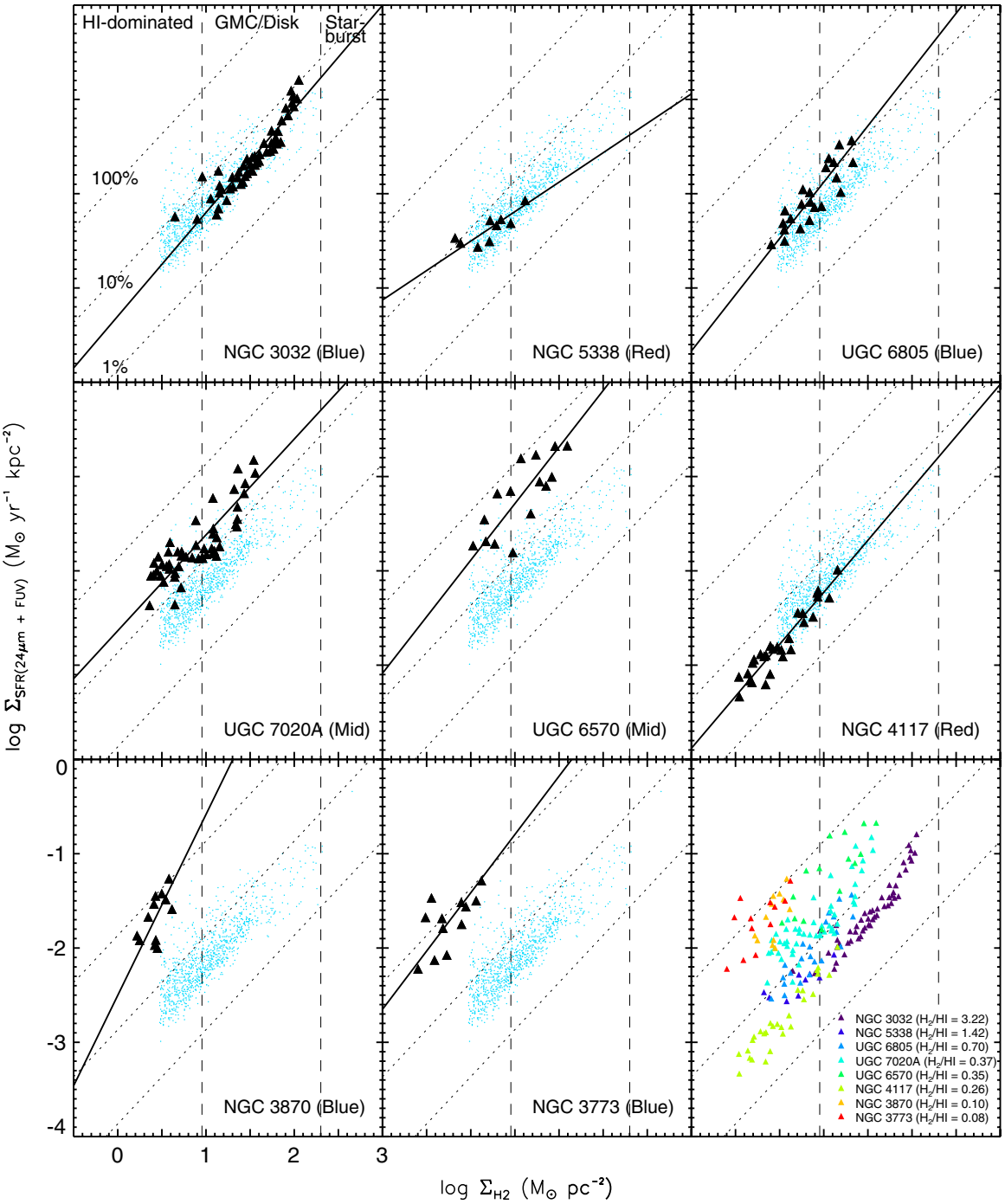

Figure 2. $\Sigma_{\rm SFR}$ vs. $\Sigma_{\rm H_2}$ at 750 pc resolution. Points for the seven spirals from Bigiel et al. (2008) are plotted in light blue. Black triangles show our eight E/S0s resolved in CO(1–0) with CARMA. Vertical dashed lines demarcate the three different regimes of star formation discussed in Bigiel et al. (2008) and dotted lines mark constant MSFE, corresponding (from top to bottom) to the depletion of 100%, 10%, and 1% of the molecular gas (including helium) within 10^8 yr, or equivalently to molecular gas depletion timescales of 0.1, 1, and 10 Gyr. Solid black lines represent OLS bisector fits. The color sequence (blue/mid/red) is noted at the bottom of each panel. The last panel combines the points for all eight galaxies, color coded by $M_{\rm H_2}/M_{\rm H\,I}$, illustrating variations in MSFE with power-law index N and $M_{\rm H_2}/M_{\rm H\,I}$ (see Sections 3 and 5).

Figure 3 also shows a similarly large spread in aperture-averaged MSFEs as seen for local MSFEs in Section 3, with over half of the CARMA-detected and all of the 30 m observed E/S0s (all blue- or mid-sequence) offset toward apparently higher MSFEs (>10%) compared to the typical spirals from Bigiel et al. (2008). Equivalently, the molecular gas depletion times for our E/S0s range from 2.3 down to 0.1 Gyr, with a median of 0.5 Gyr—lower than that of the Bigiel et al. spirals. Additionally, the offset toward apparently higher MSFEs is seen in both the CARMA and IRAM 30 m galaxies in Figure 3, so it is not specific to interferometric data.

5. DISCUSSION

We have shown above that the relationship between molecular gas and star formation in low-mass E/S0s ($M_* \lesssim 4 \times 10^{10}\,M_\odot$) resolved at 750 pc is similar to that for spirals, with a roughly linear correlation between $\Sigma_{\rm H_2}$ and $\Sigma_{\rm SFR}$ all the way down to the

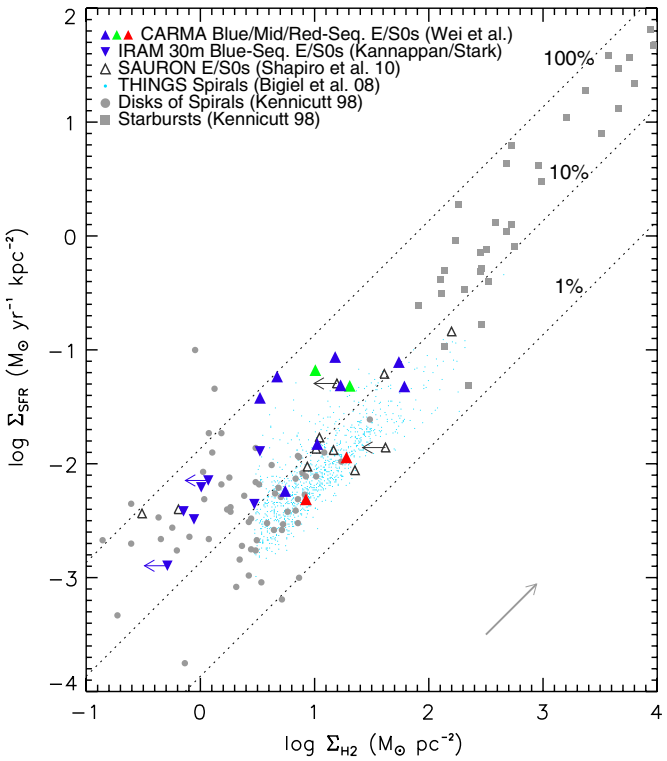

Figure 3. Aperture-averaged Σ_{SFR} vs. Σ_{H_2} for normal disk and nuclear starburst galaxies from Kennicutt (1998), SAURON E/S0s from Shapiro et al. (2010), and E/S0s from this Letter. The 750 pc resolution points from Bigiel et al. (2008) are also plotted in the background for comparison. Dotted lines mark the same lines of constant MSFE as in Figure 2. Gray arrow in the lower right shows typical shift of spiral disk points from Kennicutt (1998) if averaged over 0.6 R_{25} instead of R_{25}.

H I-dominated regime. This suggests that star formation occurs in H_2 and not H I, similar to what Bigiel et al. (2008) find for spirals. One intriguing difference is the apparently elevated MSFEs of our E/S0s compared to the MSFEs of the Bigiel spirals. *Star formation efficiency*, however, may be a misnomer in some cases, as other factors may contribute to the observed offsets.

One possible cause for apparently elevated MSFEs is that the CO may not trace all of the H_2 in these galaxies, as many are low-mass systems where X_{CO} may be variable (e.g., Maloney & Black 1988; Pak et al. 1998; Pelupessy & Papadopoulos 2009). Kennicutt (1998) finds a similar scatter in MSFEs for low-luminosity ($L_B < 10^{10}\,L_\odot$) disk galaxies, which he attributes to variation in X_{CO}, possibly due to low metallicities. Recent *Herschel* results support this, finding evidence for excess cold dust that is not well traced by CO in low-mass galaxies (O'Halloran et al. 2010; Kramer et al. 2010). However, metallicity measurements (available for 5/6 CARMA-detected and 3/7 IRAM-observed galaxies offset toward higher MSFEs) indicate that these galaxies are well within the range ($\gtrsim$1/4 $Z_\odot$) where much work suggests that X_{CO} is similar to that assumed here (e.g., Rosolowsky et al. 2003; Leroy et al. 2006; Wolfire et al. 2010).

A second explanation is that some of these galaxies are advanced, H_2-depleted starbursts, where the delay between H_2 exhaustion and fading of star formation tracers associated with young, massive stars gives the *appearance* of elevated MSFEs. Thus, the possible correlation between elevated MSFE, lower $M_{H_2}/M_{H\,I}$, and steeper (higher N) slopes in the Schmidt–Kennicutt relation found in Section 3 may reflect the depletion of H_2 in the later stages of star formation, in good agreement with simulations that predict steeper Schmidt–Kennicutt relations and higher MSFEs as the molecular gas fraction decreases (Robertson & Kravtsov 2008). This is consistent with studies of NGC 1569, a post-starburst dwarf irregular (e.g., Angeretti et al. 2005) that also appears to have an elevated MSFE (Leroy et al. 2006).

A third possibility is that the observed offsets may reflect truly enhanced MSFEs. Kannappan & Wei (2008), updating Kannappan (2004), find that the fractional gas content of galaxies abruptly rises below a gas-richness threshold mass of $M_* \sim$ (3–5) $\times\ 10^9\,M_\odot$, roughly corresponding to internal velocities of $\sim$120 km s^{-1} (see also KGB). This is the same velocity threshold below which the physics of star formation may change due to possibly increased gas accretion, outflow, and metal loss from shallower potentials (Dalcanton et al. 2004; Garnett 2002; Dalcanton 2007). While the *total* SFEs of dwarf galaxies are low compared to those of normal star-forming spirals (e.g., Hunter & Elmegreen 2004; Dalcanton et al. 2004; Dalcanton 2007; Robertson & Kravtsov 2008), recent simulations suggest that gas-rich and/or lower metallicity galaxies deviate from the Schmidt–Kennicutt relationship toward higher *molecular* SFEs (Pelupessy & Papadopoulos 2009). These predictions are supported by observations of local dwarfs, which find high MSFEs in IC 10 and M33 compared to nearby spirals (Leroy et al. 2006; Gardan et al. 2007). This phenomenon could contribute to the scatter in MSFEs observed by Kennicutt (1998), as $L_B \sim 10^{10}\,L_\odot$ roughly corresponds to the gas-richness threshold mass. Similarly, the two SAURON E/S0s in Figure 3 with the highest MSFEs are low-luminosity systems with $L_B < 10^{10}\,L_\odot$.

Unlike previous studies of star formation in blue E/S0s, our sample focuses on galaxies below the gas-richness threshold mass (13 of our 19 E/S0s). At higher stellar masses, AGN and strong starbursts are observed to dominate the blue E/S0 population (e.g., Schawinski et al. 2009; Lee et al. 2010), which is not inconsistent with the nature of our six higher-mass E/S0s (three known/candidate AGNs and two likely starbursts[5]).

Our results suggest that (possibly milder) bursts likely play a key role for lower-mass E/S0s as well. The variation of MSFE in this scenario has implications for our understanding (and theoretical simulations) of low-mass galaxy evolution. The dynamical timescales for gas inflow typical for our sample (0.06–0.4 Gyr; Wei et al. 2010) are short compared to the molecular gas consumption times we find here (0.1–2.3 Gyr), which suggests that refueling of H_2 from the H I reservoir to sustain star formation is limited only by the frequency of minor mergers/interactions that trigger gas inflow. If apparently elevated MSFEs reflect advanced, H_2-depleted bursts, the fact that 15 of our 19 E/S0s have MSFE >10% suggests that low-mass E/S0s may experience frequent small starbursts (with the caveat that we have sampled the most strongly star-forming examples by favoring blue-sequence E/S0s detected in CO). Therefore, the TSFEs of lower-mass galaxies, when time averaged over many bursts, may be elevated—consistent with the KGB finding that the concentration indices in blue-sequence E/S0s are similar to those identified by Kauffmann et al. (2006) as optimal for peak time-averaged TSFE. Our results support the

[5] UGC 12265N and UGC 6003 do not appear in the starburst regime of Figure 3 due to their large distances and the resulting poor resolution of the central region, but their nuclear EW(Hα) emission measurements (86 Å and 76 Å, respectively) and very blue-centered color gradients suggest recent/ongoing central starbursts.

picture of KGB and Wei et al. (2010) that many blue-sequence E/S0s are in a "sweet spot" with abundant gas and bursty star formation enabling efficient disk building.

We thank the referee for helpful comments, A. Leroy for sharing the THINGS data and for useful discussions, and S. Jogee for her role in acquiring the *Spitzer* data. We are grateful to A. Bolatto, J. Gallimore, M. Lacy, A. Moffett, M. Thornley, and S. Veilleux for insightful conversations. This work is based in part on observations made with the *Spitzer Space Telescope*, which is operated by JPL, Caltech under a contract with NASA. Support for this work was provided by NASA through an award issued by JPL/Caltech. This work uses observations made with the NASA Galaxy Evolution Explorer. *GALEX* is operated for NASA by Caltech under NASA contract NAS5-98034. We acknowledge support from the *GALEX* GI grant NNX07AT33G. CARMA development and operations are supported by NSF under a cooperative agreement, and by the CARMA partner universities.

REFERENCES

Angeretti, L., Tosi, M., Greggio, L., Sabbi, E., Aloisi, A., & Leitherer, C. 2005, AJ, 129, 2203
Bigiel, F., Leroy, A., Walter, F., Brinks, E., de Blok, W. J. G., Madore, B., & Thornley, M. D. 2008, AJ, 136, 2846
Combes, F., Young, L. M., & Bureau, M. 2007, MNRAS, 377, 1795
Crocker, A. F., Bureau, M., Young, L. M., & Combes, F. 2010, MNRAS, 1660
Dalcanton, J. J. 2007, ApJ, 658, 941
Dalcanton, J. J., Yoachim, P., & Bernstein, R. A. 2004, ApJ, 608, 189
Gardan, E., Braine, J., Schuster, K. F., Brouillet, N., & Sievers, A. 2007, A&A, 473, 91
Garnett, D. R. 2002, ApJ, 581, 1019
Gordon, K. D., Engelbracht, C. W., Rieke, G. H., Misselt, K. A., Smith, J., & Kennicutt, R. C., Jr. 2008, ApJ, 682, 336
Hunter, D. A., & Elmegreen, B. G. 2004, AJ, 128, 2170
Jansen, R. A., Fabricant, D., Franx, M., & Caldwell, N. 2000, ApJS, 126, 331
Kannappan, S. J. 2004, ApJ, 611, L89
Kannappan, S. J., Guie, J. M., & Baker, A. J. 2009, AJ, 138, 579
Kannappan, S. J., & Wei, L. H. 2008, in AIP Conf. Ser. 1035, The Evolution of Galaxies Through the Neutral Hydrogen Window, ed. R. Minchin & E. Momjian (Melville, NY: AIP), 163
Kauffmann, G., Heckman, T. M., De Lucia, G., Brinchmann, J., Charlot, S., Tremonti, C., White, S. D. M., & Brinkmann, J. 2006, MNRAS, 367, 1394
Kennicutt, R. C., Jr. 1998, ApJ, 498, 541
Kennicutt, R. C., Jr., et al. 2007, ApJ, 671, 333
Kewley, L. J., Groves, B., Kauffmann, G., & Heckman, T. 2006, MNRAS, 372, 961
Kramer, C., et al. 2010, A&A, 518, L67
Kroupa, P. 2001, MNRAS, 322, 231
Krumholz, M. R., McKee, C. F., & Tumlinson, J. 2009, ApJ, 699, 850
Lee, J. H., Hwang, H. S., Lee, M. G., Lee, J. C., & Matsuhara, H. 2010, ApJ, 719, 1946
Leroy, A., Bolatto, A. D., Simon, J. D., & Blitz, L. 2005, ApJ, 625, 763
Leroy, A., Bolatto, A., Walter, F., & Blitz, L. 2006, ApJ, 643, 825
Leroy, A. K., Walter, F., Brinks, E., Bigiel, F., de Blok, W. J. G., Madore, B., & Thornley, M. D. 2008, AJ, 136, 2782
Maloney, P., & Black, J. H. 1988, ApJ, 325, 389
Murray, N. 2009, ApJ, 691, 946
O'Halloran, B., et al. 2010, A&A, 518, L58
Pak, S., Jaffe, D. T., van Dishoeck, E. F., Johansson, L. E. B., & Booth, R. S. 1998, ApJ, 498, 735
Pelupessy, F. I., & Papadopoulos, P. P. 2009, ApJ, 707, 954
Robertson, B. E., & Kravtsov, A. V. 2008, ApJ, 680, 1083
Rosolowsky, E., Engargiola, G., Plambeck, R., & Blitz, L. 2003, ApJ, 599, 258
Sage, L. J., Welch, G. A., & Young, L. M. 2007, ApJ, 657, 232
Sajina, A., Lacy, M., & Scott, D. 2005, ApJ, 621, 256
Sault, R. J., Teuben, P. J., & Wright, M. C. H. 1995, in ASP Conf. Ser. 77, Astronomical Data Analysis Software and Systems IV, ed. R. A. Shaw, H. E. Payne, & J. J. E. Hayes (San Francisco, CA: ASP), 433
Schawinski, K., et al. 2009, ApJ, 690, 1672
Shapiro, K. L., et al. 2010, MNRAS, 402, 2140
Temi, P., Brighenti, F., & Mathews, W. G. 2007, ApJ, 660, 1215
Thronson, H. A., Jr., Tacconi, L., Kenney, J., Greenhouse, M. A., Margulis, M., Tacconi-Garman, L., & Young, J. S. 1989, ApJ, 344, 747
Wei, L. H., Kannappan, S. J., Vogel, S. N., & Baker, A. J. 2010, ApJ, 708, 841
Welch, G. A., & Sage, L. J. 2003, ApJ, 584, 260
Wolfire, M. G., Hollenbach, D., & McKee, C. F. 2010, ApJ, 716, 1191
Wong, T., & Blitz, L. 2002, ApJ, 569, 157
Young, L. M., Bendo, G. J., & Lucero, D. M. 2009, AJ, 137, 3053